Article:
Lalwani, V., Sharma, P., Pruncu, C.I. et al. (2020) Response surface methodology and artificial neural network-based models for predicting performance of wire electrical discharge machining of inconel 718 alloy. Journal of Manufacturing and Materials Processing, 4 (2). 44.

https://doi.org/10.3390/jmmp4020044

Journal of
Manufacturing and Materials Processing

MDPI

Article

Response Surface Methodology and Artificial Neural Network-Based Models for Predicting Performance of Wire Electrical Discharge Machining of Inconel 718 Alloy

Vishal Lalwani [1], Priyaranjan Sharma [2], Catalin Iulian Pruncu [3,4,*] and Deepak Rajendra Unune [1,5]

1 Department of Mechanical-Mechatronics Engineering, The LNM Institute of Information Technology, Jaipur-302031, India; vishallalwani121@gmail.com (V.L.); deepunune@gmail.com (D.R.U.)
2 Department of Mechanical Engineering, National Institute of Technology, Karnataka, Surathkal-575025, India; priya333ranjan@gmail.com
3 Mechanical Engineering, Imperial College London, Exhibition Rd., London SW7 2AZ, UK
4 Mechanical Engineering, School of Engineering, University of Birmingham, Birmingham B15 2TT, UK
5 Department of Materials Science and Engineering, INSIGNEO Institute of in silico Medicine, University of Sheffield, Sir Robert Hadfield Building, Mappin Street, Sheffield S1 3JD, UK
* Correspondence: c.pruncu@imperial.ac.uk

Received: 7 April 2020; Accepted: 1 May 2020; Published: 6 May 2020

Abstract: This paper deals with the development and comparison of prediction models established using response surface methodology (RSM) and artificial neural network (ANN) for a wire electrical discharge machining (WEDM) process. The WEDM experiments were designed using central composite design (CCD) for machining of Inconel 718 superalloy. During experimentation, the pulse-on-time (T_{ON}), pulse-off-time (T_{OFF}), servo-voltage (SV), peak current (I_P), and wire tension (WT) were chosen as control factors, whereas, the kerf width (Kf), surface roughness (R_a), and materials removal rate (MRR) were selected as performance attributes. The analysis of variance tests was performed to identify the control factors that significantly affect the performance attributes. The double hidden layer ANN model was developed using a back-propagation ANN algorithm, trained by the experimental results. The prediction accuracy of the established ANN model was found to be superior to the RSM model. Finally, the Non-Dominated Sorting Genetic Algorithm-II (NSGA- II) was implemented to determine the optimum WEDM conditions from multiple objectives.

Keywords: response surface method (RSM); artificial neural network (ANN); wire electrical discharge machining (WEDM); kerf width (Kf); surface roughness (R_a); material removal rate (MRR), NSGA-II

1. Introduction

For the past few decades, Inconel 718 alloy has been widely employed for the manufacturing of critical aircraft components owing to its high strength at elevated temperature, good corrosion resistance, and excellent fatigue resistance [1,2]. Due to superior thermal, chemical, and mechanical properties, the traditional machining of Inconel 718 typically results in the formation of built-up-edge at elevated temperature. It weakens the degradation of the machining performances, thereby the literature has endorsed it as a difficult-to-cut material [1,2]. The problems of machining of difficult-to-cut materials can be minimised by using the non-traditional machining techniques. Wire electrical discharge machining (WEDM) can be effectively used for the machining of difficult-to-cut materials and has the ability to produce accurate, precise, and complex surfaces with the help of very thin wires [3,4]. However, the selection of the proper machining parameters to achieve the desired machining performance has always been a challenging task for industry [5].

WEDM is an electro-thermal machining process in which a rapid cyclic spark yields a temperature around 10,000 °C. It is discharged in the gap between an electrically conductive wire electrode and the work piece that further leads to material removal through melting and evaporation [6]. This process is governed by several direct and indirect parameters such as pulse-on-time, pulse- off-time, peak current, wire tension, gap voltage, frequency of discharge, mechanical and thermal properties of wire electrode, and work piece, etc. Most researchers have presented their studies on the influence of input parameters of WEDM on various responses including and materials removal rate (MRR), kerf width, and surface roughness, etc. Tosun et al. [7] applied Taguchi's approach to perform experiments during the machining of AISI4140 steel to investigate the impact of pulse duration, open circuit voltage, wire speed, and dielectric flushing pressure on MRR and kerf width. They concluded that the open circuit voltage and pulse duration have a significant impact on MRR and kerf width in the WEDM process. Hewidy et.al. [8] applied the response surface methodology (RSM) approach during the machining of Inconel 601, where they highlighted the impact of peak current, duty factor, wire tension, and water pressure on the MRR, wear ratio and surface roughness. It has been reported that peak current increases the MRR and wear ratio while decreasing the surface finish owing to increased discharge energy. In [9], the authors used the Genetic Algorithm (GA) for multipurpose optimization of WEDM and examined the effects of different process parameters like discharge current, pulse duration, pulse frequency, wire speeds, wire tension, and dielectric flow rate on MRR, surface roughness (R_a), and kerf width (K_f). Further, Kumar and Agarwal [10] applied the NSGA-II optimization method to optimize WEDM input parameters for multi-objective optimization of surface integrity and MRR while performing high speed machining of steel with the help of zinc coated wire. The literature survey shows that many studies have already reported on WEDM processes for the machining of titanium alloys. Constrained and Pareto optimization techniques were used for the optimization of WEDM for various process parameters like dimensional deviation, cutting speed, and surface integrity during the machining of c-titanium aluminide alloy by Sarkar et al. [11]. In other study, Kuriakose et al. [12] used zinc coated brass wire for the machining of titanium alloy (Ti-6Al-4V). They further studied the effects of numerous process variables using the machine learning based data mining method on cutting speed and surface integrity. Manna and Bhattacharyya [13] used the Gauss elimination dual response technique in order to find the optimum machining conditions for WEDM during the machining of aluminium reinforced silicon carbide metal matrix composites. WEDM for the machining of Armor materials was presented by Bobbili et al. [14] to machine RHA steel and aluminium alloy 7017. They concluded that an increase in pulse-on-time increases MRR and surface roughness. Patil and Brahmankar [15] investigated the effects of various WEDM process parameters on surface quality, kerf width, and cutting speed using brass wire material with a zinc coating. They applied Taguchi's approach for the machining of alumina particulate reinforced aluminium matrix composites (Al/Al_2O_3p). They recommended that current, and pulse-on-time have substantial influence on cutting rate, surface finish, and kerf width.

It was found that designing a mathematical relationship between the input process parameters and the output responses is extremely difficult in WEDM because of the inherent nonlinear nature of these process parameters [16]. In order to find the responses for a given set of process parameters and to optimize them, the modelling of a complex system is crucial for reducing the manufacturing costs. From the literature survey, we found that artificial neural network (ANN) is a widely used technique for process modelling and optimization. This is because of its ability to form non-linear relations between various inputs and output parameters. Further, it can be easily applied for modelling complex problems owing to its powerful data-driven, self-adaptive, flexible computational capabilities, unlike mathematical models. Moreover, ANN can handle large quantity of data sets for training and has the ability to implicitly detect complex nonlinear relationships between dependent and independent variables. The research work conducted by Samantha et al. [17] investigated the predicted values for both ANN and the regression model. The performance of these two approaches was compared and ANN was found to be more efficient. Biswas et al. [18] found that ANN architecture is a unique, flexible, and powerful method of modelling for the laser micro-drilling process on titanium nitride/alumina composites. Table 1 presents a comprehensive review of the literature on the application of ANN for modelling of the WEDM process.

Table 1. Previous research on application of ANN in modelling WEDM.

Author(s)	Prediction Model	Training Method	Work Piece	Machining Parameters	Response Variables	Summary
Ramakrishnan and Karunamoorthy [19]	feedforward neural network	-	Inconel 601	T_{ON}, delay time, wire feed rate, ignition current	MRR, R_a	T_{ON} found to be most imfluecing factor for MRR.
Saha et al. [20]	feed-forward back-propagation neural network with 1-hidden layer	-	tungsten carbide-cobalt (WC-Co) composite	T_{ON}, T_{OFF}, I_P, capacitance	Cutting speed, R_a	ANN predicts MRR & R_a with 3.29% overall mean prediction error.
Khan and Rajput [21]	feed-forward back-propagation neural network	-	Alloy Steel (HCHCr)	T_{ON}, T_{OFF}, I_P, average gap voltage, WT, Wire feed	Cutting speed, R_a	Higher cutting speed degrades surface finish.
Shandilya and Jain [22]	Back-propagation neural network with 1-hidden layer	-	SiCp/6061 Al metal matrix composite	T_{ON}, T_{OFF}, voltage, wire feed	Surface roughness	ANN model outperforms RSM model prediction.
Zhang et al. [23]	BPNN with 2-hidden layers	-	SKD11 steel	T_{ON}, T_{OFF}, I_P, wire speed, tracking coefficient	Cutting speed, R_a, MRR	T_{ON}, T_{OFF} are significant factors for R_a.
Ugrasen et al. [24]	BPNN with 1-hidden layer	Levenberg-Marquardt	-	T_{ON}, pulse-off-time, I_P, bed speed	VMRR, accuracy, R_a	ANN model with 70% training data gave best prediction as that of model with 50% or 60% training data.
Vates et al. [25]	ANN with 1-hidden layer	-	D2 Steel	gap voltage, flush rate, T_{ON}, T_{OFF}, wire feed, and WT	R_a, MRR	Best surface finish achieved at lower MRR values.
Shakeri et al. [26]	Feedforward backpropagation neural network	Levenberg-Marquardt	cementation alloy steel	wire speed, servo speed, frequency, I_P	R_a, MRR	ANN model outperformed Regression models prediction.
Jafari et al. [27]	ANN with 1-hidden layer	Bayesian regularization	Copper	T_{ON}, T_{OFF}, I_P, spark gap voltage, wire speed	R_a	I_P had most significant effect of Ra followed by T_{ON}.
Singh and Mishra [28]	BPNN with 1-hidden layer	Levenberg-Marquardt	Nimonic 263	T_{ON}, T_{OFF}, I_P, spark gap voltage	R_a, recast layer thickness	
Mukhopadhyay et al. [29]	feedforward neural network	Levenberg-Marquardt	EN 31 tool steel	Discharge current, SV, T_{ON}, T_{OFF}	fractal dimension	

From Table 1, it can be seen that most of the work carried out in the past did not consider the superalloys, especially, Inconel 718, as the work piece. The kerf width is a critical response parameter for the WEDM process which influences the accuracy of the WEDM operation, but was not considered in previous studies while modelling the WEDM process. That apart, most of the work used single hidden based ANN architecture and the prediction accuracy of the developed model has not been critically examined.

Therefore, the aim of this work was to perform a systematic investigation while machining Inconel 718 using WEDM operation and to establish an accurate ANN-based prediction model for the process. MRR, R_a, and kerf width were selected as performance measures for the varying input parameters, viz., pulse-on-time (T_{ON}), pulse-off-time (T_{OFF}), servo-voltage (SV), peak current (I_P), and wire tension (WT). Moreover, the performance of the established ANN model was compared with the traditional RSM model. Initially, the central composite design (CCD) approach was used to develop the experimental plan. Then, based on the experimental results, the ANN and RSM models were established and their performance compared. Further, the machining characteristics were evaluated using the established ANN model. Finally, The Non-dominated Sorting Genetic Algorithm (NSGA-II) was applied for optimisation of WEDM process performance.

2. Experimentation

2.1. Workpiece Material

The work piece specimens of size 50 mm $(length) \times 12$ mm$(width) \times 2.5$ mm$(height)$ were prepared from commercial Inconel 718 material with the help of an abrasive cutter (Isomet-4000, Buehler, Lake Bluff, IL, USA). To obtain a uniform surface finish, the specimens were finished using a semi-automatic polishing-machine (MetaServ-250, Buehler, Lake Bluff, IL, USA). The composition of the work piece was investigated using a glow discharge spectrometer (GDS-500A, LECO, Saint Joseph, MI, USA) and the results are shown in Table 2.

Table 2. Chemical composition of our work piece material (Inconel 718).

Component	Ni	C	Si	Mn	P	Cr	Fe	Mo
Weight %	55.40	00.03	00.08	00.04	00.01	23.80	03.70	13.30
Component	V	Nb	W	Co	Ti	Al	Zr	
Weight %	00.09	02.78	00.26	00.26	00.81	00.19	00.08	

2.2. Experimental Setup

The experimental layout is shown in Figure 1. The experiments were conducted using a CNC Wire-EDM machine (Ecocut, Electronica, Pune, India). A cylindrical brass wire (Ø 250 µm) was used as a wire electrode with negative polarity and deionized water was used as the dielectric fluid. Both electrodes were kept immersed in dielectric without any external flushing while performing experiments.

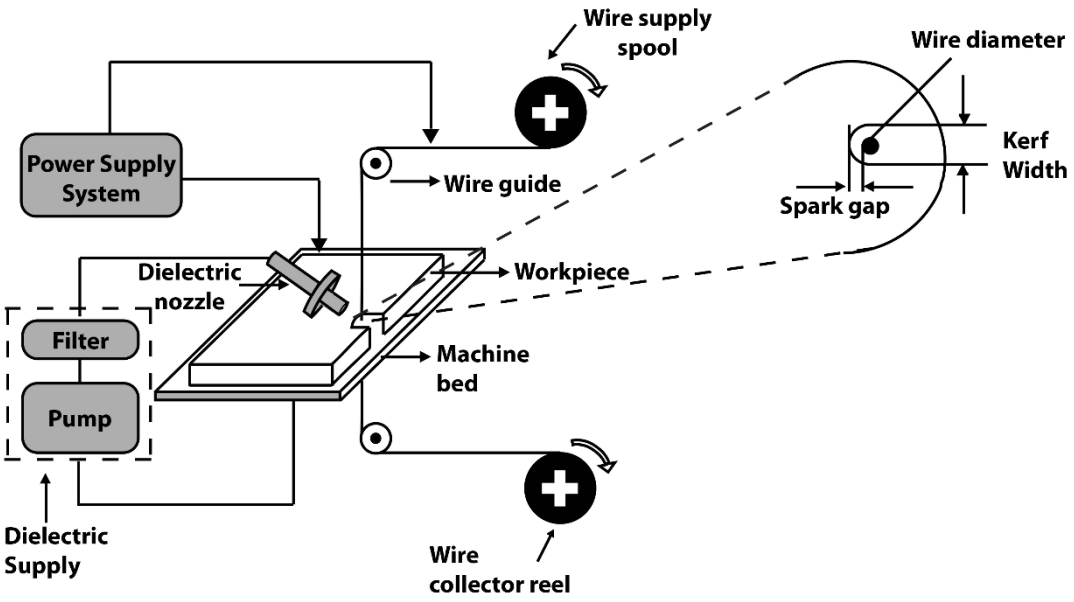

Figure 1. Schematic diagram of the wire electrode discharge machining (WEDM).

For WEDM operation, the important variables having significant impact on the response variable are the electrical parameters, diameter and tension of wire, electrical and physical properties of the wire, and work piece materials. For this research, the aim was to analyse the effect of electrical parameters for selected brass wire (Ø 250 µm) and Inconel 718 work piece alloy so that industry can select suitable machining parameters to achieve the desired performance. Therefore, the pulse- on-time (T_{ON}), pulse-off-time (T_{OFF}), servo-voltage (SV), peak current (I_P), and wire tension (WT) were selected as the input machining parameters. The input parameters and their levels are shown in Table 3. The current levels of input parameter were chosen based on the literature review, trial runs, mechanism competence, and machine constraints.

Table 3. Independent control factors, and their levels.

Input Parameter	Symbol	Unit	Level		
			−1	0	1
pulse-on-time	T_{ON}	µs	100	110	120
pulse-off-time	T_{OFF}	µs	40	50	60
servo-voltage	SV	V	40	50	60
peak current	I_P	A	120	150	180
wire tension	WT	kg	1.1	1.3	1.5

In WEDM technology, each pulse is associated with on-time and off-time expressed in microseconds (µs). Upon dielectric breakdown, current commences flowing and the period for which current flows to the end of the discharge is known as pulse-on-time (T_{ON}). The period between two consecutive pulses is generally known as pulse-off-time (T_{OFF}). This period is time lapsed from the end of a discharge to the start of consecutive discharge. During pulse-off-time, WEDM remains at momentary rest and deionization of plasma resulting from previous discharge takes place [30]. The servo motion of EDM is controlled harmony with gap-voltage fluctuation relative to SV. The wire electrode advances in the machining direction when the gap voltage is higher than SV or else the wire electrode is retracted backwards. The maximum current accessible for each pulse during a spark that is applied between both electrodes is known as the peak current. It is an important parameter that is widely considered in EDM technology. Apart from the above mentioned electrical parameters, the wire tension is considered a crucial parameter which can affect cutting accuracy and profile shape [31].

The kerf width (K_f), surface roughness (R_a), and material removal rate (MRR) were chosen as the response variables. An optical microscope (AxioCam AX10, Zeiss, Germany) was used for the measurement of kerf width at five different locations along the length of the microchannel (as shown in Figure 2) and then the average of these measurements was considered as K_f of the microchannel. R_a was measured at three different locations on the same surface using a surface roughness tester (SJ210, Mitutoyo, Japan) which has a conformance standard of ISO 1997 and the corresponding mean value was considered as the net R_a value. The cut-off length (λ_c) of 0.8 mm and the number of sampling (λ) of five (traverse length is $0.8 \times 5 = 4$ mm) were used in the measurements. Furthermore, the surface quality was investigated by analysing the surface morphology with the help of field emission electron scanning microscopic (FESEM) images taken by Nova NanoSEM 450® (FEI, Hillsboro, OR, USA).

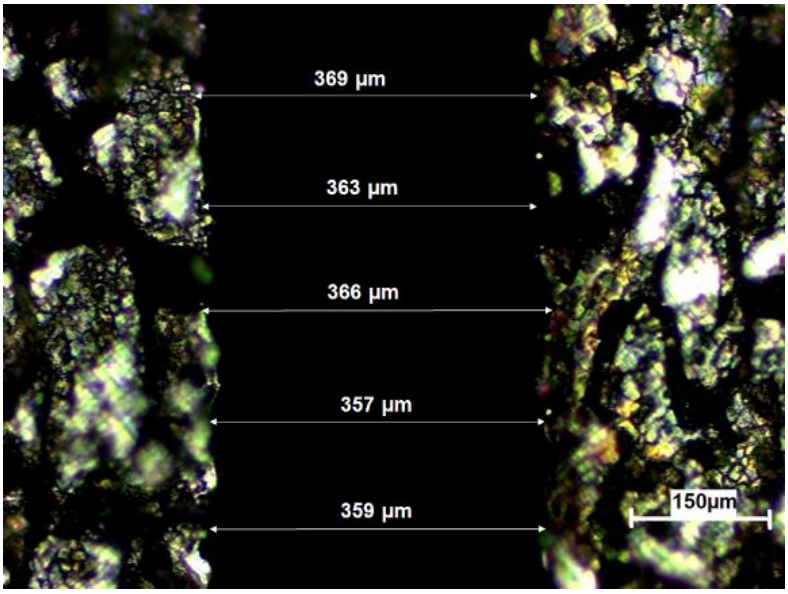

Figure 2. Kerf width measurement using an optical microscope.

2.3. Response Surface Methodology (RSM)

RSM is a combination of statistical and mathematical methods for prediction and optimization of response parameters which include quantifiable independent variables [32]. The WEDM system is described by a second order (quadratic) polynomial model:

$$Y = \alpha_0 + \sum_{i=1}^{n} \alpha_i X_i + \sum_{i=1}^{n} \alpha_{ii} X_i^2 + \sum_{i=1}^{n} \sum_{j=1}^{n} \alpha_{ij} X_i X_j \quad (1)$$

where Y represents the predicted response variable, α_0, α_i, *and* α_{ii} represent constant term, linear coefficients and quadratic coefficients, respectively. The cross-product coefficients are represented by α_{ij}, the total number of factors and input parameters are represented by n and X, respectively.

In the current study, the experiments were planned on the basis of central composite design (CCD) which is a well-known design methodology within response surface methodology. The CCD technique reduces the total number of experimental trials essential to evaluate the effects of each parameter and its interactions [33]. The face-cantered design with eight centre points was selected for investigation and measured response values are shown in Table 4.

Table 4. Experimental plan with chosen input machining parameters and measured response variables.

S. No.	Input Machining Parameters					Response Variables		
	Pulse on Time (μs)	Pulse off Time (μs)	Servo Voltage (V)	Peak current (A)	Wire Tension (kg)	Kerf Width (mm)	Average Surface Roughness (μm)	MRR (mm^3/min)
1	120	40	60	120	1.1	0.402	3.71	10.53
2	100	40	40	180	1.1	0.382	1.71	05.28
3	100	60	40	120	1.1	0.350	1.52	02.39
4	120	60	60	120	1.1	0.385	3.77	09.04
5	110	40	50	150	1.3	0.399	1.51	08.34
6	120	60	60	120	1.5	0.404	3.58	08.18
7	120	50	50	150	1.3	0.416	3.51	08.19
8	100	40	40	120	1.1	0.356	1.75	04.64
9	120	60	40	180	1.5	0.404	3.81	05.85
10	110	50	50	150	1.5	0.395	2.86	07.91
11	100	40	60	120	1.5	0.369	1.27	06.53
12	120	60	40	120	1.5	0.411	3.38	05.58
13	120	60	40	120	1.1	0.391	3.55	05.38
14	120	40	60	180	1.1	0.433	3.09	10.22
15	100	60	60	180	1.1	0.361	1.74	05.14
16	110	50	50	120	1.3	0.386	2.27	06.68
17	100	50	50	150	1.3	0.365	1.61	04.19
18	120	40	60	120	1.5	0.433	2.87	10.36
19	120	40	40	120	1.1	0.397	3.35	07.38
20	110	50	50	150	1.3	0.392	2.60	07.96
21	110	50	50	150	1.3	0.378	2.52	07.54
22	100	60	60	120	1.1	0.350	1.70	04.91
23	100	60	60	120	1.5	0.337	1.51	04.78
24	120	40	40	180	1.5	0.411	3.51	07.78
25	100	40	40	120	1.5	0.366	1.55	04.94
26	100	40	60	120	1.1	0.349	1.48	06.36
27	120	40	60	180	1.5	0.426	3.30	10.80
28	120	60	60	180	1.5	0.407	4.00	08.85
29	100	60	40	180	1.1	0.368	1.54	03.47
30	100	60	40	120	1.5	0.360	1.32	02.69
31	110	50	50	150	1.3	0.392	2.59	07.35
32	120	60	60	180	1.1	0.414	3.80	08.95
33	110	50	50	180	1.3	0.402	2.49	07.33
34	100	40	60	180	1.1	0.381	1.53	05.19
35	100	60	60	180	1.5	0.359	1.91	05.64
36	110	50	50	150	1.3	0.391	2.59	07.44
37	110	50	50	150	1.3	0.385	2.91	07.96
38	110	60	50	150	1.3	0.387	2.28	06.41
39	110	50	50	150	1.3	0.392	2.64	07.41
40	100	40	60	180	1.5	0.366	1.91	06.79
41	100	40	40	180	1.5	0.370	1.20	05.38
42	120	40	40	120	1.5	0.407	3.14	07.33
43	110	50	50	150	1.3	0.402	2.59	07.16
44	110	50	60	150	1.3	0.394	3.00	08.92
45	120	40	40	180	1.1	0.419	3.36	07.18
46	110	50	50	150	1.3	0.392	2.56	07.40
47	120	60	40	180	1.1	0.410	3.69	04.82
48	110	50	50	150	1.1	0.392	2.15	08.77
49	100	60	40	180	1.5	0.378	1.71	03.83
50	110	50	40	150	1.3	0.420	3.51	08.26

2.4. Artificial Neural Network (ANN)

ANN is an intelligent computational system able to fit complex functions. It was successfully used for solving numerous problems in various fields such as diagnosing of faults, identification of the process, property estimation, smoothing of data, and error filtering, designing and development of a product, optimization of processes, and estimation of activity coefficients [34,35]. The neural network is based on the idea of biological neural networks, and can be defined as a vastly parallel distributed processing technique. It is formed by neurons that have the capability to acquire, to learn, and to adapt to the information, in order to make it available for future use [36,37]. Thus, by taking the computational capability of a multi-layered neural network into account, we adopted it for the modelling of the WEDM process to predict the response variables K_f, R_a, and MRR involved in the machining of Inconel 718.

2.5. Non-Dominated Sorting Genetic Algorithm (NSGA-II)

The NSGA-II was chosen to optimize WEDM using the developed mathematical models. The reason is linked to the complexity nature of the WEDM process because it assumes three

objectives to be solved all together. Thus, it can be extremely difficult to determine the optimal solution for the WEDM. In single-objective optimization, the best decision is usually obtained by determining the global maxima/global minima depending on the nature of the optimization problem. While in the case of multiple objectives optimization, there exists more than one solution. There are a number of classical techniques available to determine the solutions of a multi-objective problem such as min– max, distance function, and weighted sum techniques. However, these methods have several disadvantages like weighing of objectives based on their relative importance. The authors must have complete knowledge of the ranking of objective functions while using conventional optimization methods. While using Genetic Algorithm based techniques, users do not require any gradient information and inherent parallelism in searching the design space, thus making it a robust adaptive optimization technique. NSGA-II was designed based on the Pareto methodology and it has been established as a competent algorithm for cracking any multiple optimization problem [38]. The fast, non-dominated sorting, fast crowded distance estimation, and simple crowded comparison operator make NSGA-II an efficient optimization technique. Basic definitions and the flow chart of NSGA-II are available in [39,40] and have not been described in this paper.

3. Results and Discussion

3.1. ANOVA Simulation

Minitab 16 software was used to execute the ANOVA for investigating the adequacy of thedeveloped models, and the results of response surface model are given in Tables 5–7 for K_f, R_a, and MRR, respectively. The backward elimination technique was used to remove the model terms which are insignificant. In the present study, all the adequacy measures, R^2, adjusted $R^{2,}$ and predicted R^2, were found to be closer to one, which implies adequacy and fit of models. The values of R^2 of 92.31% for K_f, 95.85% for R_a, and 96.30% for MRR indicate that only less than 7.59%, 4.25%, and 3.70% of the total variations in K, R_a, and MRR, respectively, were not explained by the models. The high values of the adjusted R^2 i.e., 90.57% for K_f, 94.78% for R_a and 95.10% for MRR further confirm the validity of these models. Both predicted R^2 and adjusted R^2 were found to be in conformity with each other. Lack of fit was obtained to be non-significant for each of the cases as required. The smaller value of the coefficient of variation (CV) indicates improved accuracy and consistency of the experiments performed [41].

Table 5. Results of ANOVA analysis for the kerf width (K_f).

Source	Sum of Square	Degree of freedom	Mean Square	F Value	*p*-Value Prob > F		Percentage Contribution
Model	0.024	09	2.655×10^{-3}	053.32	<0.0001	significant	
A-Pulse-on-time	0.019	01	0.019	379.94	<0.0001		73.07%
B-Pulse-off-time	1.055×10^{-4}	01	1.055×10^{-3}	021.20	<0.0001		00.40%
C-Servo Voltage	2.375×10^{-5}	01	2.375×10^{-5}	000.48	0.4938		00.09%
D-Peak Current	1.657×10^{-3}	01	1.657×10^{-3}	033.28	<0.0001		06.37%
E-Wire Tension	1.210×10^{-4}	01	1.210×10^{-4}	002.43	0.1269		00.46%
AC	3.890×10^{-4}	01	3.890×10^{-4}	007.81	0.0079		01.49%
BC	3.696×10^{-4}	01	3.696×10^{-4}	007.42	0.0095		01.42%
DE	7.443×10^{-4}	01	7.443×10^{-4}	014.95	0.0004		02.86%
A2	6.137×10^{-4}	01	6.137×10^{-4}	012.33	0.0011		02.36%
Residual	1.992×10^{-3}	40	4.979×10^{-5}				
Lack of Fit	1.654×10^{-3}	33	5.014×10^{-5}	001.04	0.5246	not significant	
Pure Error	3.371×10^{-4}	07	4.816×10^{-5}				
Cor Total	0.026	49					

σ	7.056×10^{-3}	R^2	00.923
Mean	0.39	Adjusted R^2	00.905
C.V. %	1.81	Predicted R^2	00.884
P_S	2.986×10^{-3}	Adequacy Precision	30.326

Table 6. Results of ANOVA analysis for the surface roughness (R_a).

Source	Sum of Square	Degree of Freedom	Mean Square	F Value	*p*-Value Prob > F		Percentage Contribution
Model	34.27	10	03.43	090.04	<0.0001	Significant	
A-Pulse-on-time	30.95	01	30.95	813.04	<0.0001		90.31%
B-Pulse-off-time	00.61	01	00.61	016.13	0.0003		01.77%
C-Servo Voltage	8.768×10^{-3}	01	8.768×10^{-3}	000.23	0.6339		00.02%
D-Peak Current	00.19	01	00.19	005.08	0.0300		00.55%
E-Wire Tension	00.01	01	00.01	000.28	0.5967		00.03%
AB	00.23	01	00.23	005.94	0.0195		00.67%
BC	00.11	01	00.11	002.92	0.0954		00.32%
DE	00.30	01	00.30	007.89	0.0077		00.87%
B2	01.75	01	01.75	045.97	<0.0001		05.10%
C2	01.62	01	01.62	042.51	<0.0001		04.67%
Residual	01.48	39	00.03				
Lack of Fit	01.39	32	00.04	003.11	0.0613	not significant	
Cor Total	35.76	49					
σ	0.20		R^2			00.958	
Mean	2.55		Adjusted R^2			00.947	
C.V. %	7.64		Predicted R^2			00.929	
(P_S)	2.52		Adequacy Precision			28.842	

Table 7. Results of ANOVA analysis for the material removal rate (MRR).

Source	Sum of Square	Degree of Freedom	Mean Square	F Value	*p*-Value Prob > F		Percentage Contribution
Model	184.38	12	15.37	080.17	<0.0001	significant	
A-Pulse-on-time	086.65	01	86.65	452.11	<0.0001		46.99%
B-Pulse-off-time	024.94	01	24.94	130.11	<0.0001		13.52%
C-Servo Voltage	044.77	01	44.77	233.57	<0.0001		24.28%
D-Peak Current	000.68	01	00.68	003.54	0.0678		00.36%
E-Wire Tension	000.37	01	00.37	001.92	0.1740		00.20%
AC	005.20	01	05.20	027.13	<0.0001		02.82%
BC	000.66	01	00.66	003.46	0.0707		00.35%
DE	000.76	01	00.76	003.95	0.0544		00.01%
A2	006.98	01	06.98	036.41	<0.0001		03.78%
C2	001.55	01	01.55	008.07	0.0073		00.84%
D2	001.75	01	01.75	009.13	0.0046		00.94%
E2	000.71	01	00.71	003.68	0.0628		00.38%
Residual	007.09	37	00.19				
Lack of Fit	006.51	30	00.22	002.62	0.0939	not significant	
Pure Error	000.58	07	00.08				
Cor Total	191.48	49					
σ	00.44		R^2			00.963	
Mean	06.83		Adjusted R^2			00.951	
C.V. %	06.41		Predicted R^2			00.914	
P_S	16.36		Adequacy Precision			34.899	

The significant machining parameters that affect the response variables i.e., K_f, R_a, and MRR were determined at 95% confidence level. It can be observed that the pulse-on-time (T_{ON}) is the key factor having the highest impact on K_f, R_a, and MRR, contributing 73.07% on K, 90.31% on R_a, and 46.99% on MRR, respectively. In summary, a high pulse-on-time yields a faster erosion of the material due to high values of associated discharge energy, hence a considerable increase in MRR may be observed [42].

3.2. Regression Equations

The relationships among the response characteristics (K_f, R_a, and MRR) and the input process parameters (T_{ON}, T_{OFF}, SV, I_P, and WT) were expressed by the following second-order polynomial equations in terms of actual factors.

For kerf width-

$$\begin{aligned} K \;=\; & -0.83891 + 0.017139 \times T_{ON} + 1.14203 \times 10^{-3} \times T_{OFF} - 2.21967 \times 10^{-3} \times SV + \\ & 1.27766 \times 10^{-3} \times I_P + 0.13001 \times WT + 3.48662 \times 10^{-5} \times T_{ON} \times SV \\ & -3.39838 \times 10^{-5} \times T_{OFF} \times SV - 8.03813 \times 10^{-4} \times I_P \times WT - 7.51065 \times 10^{-5} \times T_{OFF}^2 \end{aligned} \quad (2)$$

For surface roughness-

$$\begin{aligned} R_a \;=\; & -0.35667 + 0.053372 \times T_{ON} + 0.58558 \times T_{OFF} - 0.69528\ V - 0.018477 \times I_P \\ & -2.51114 \times WT + 8.40625 \times 10^{-4} \times T_{ON} \times T_{OFF} + 5.89375 \times 10^{-4} \times T_{OFF} \times SV + \\ & 0.016146 \times I_P \times WT - 6.94078 \times 10^{-3} \times T_{OFF}^2 + 6.67422 \times 10^{-3} \times SV^2\ . \end{aligned} \quad (3)$$

For MRR-

$$\begin{aligned} MRR \;=\; & -158.77725 + 3.54861 \times T_{ON} - 0.15766 \times T_{OFF} - 1.16912\ SV + 0.24375 \times I_P \\ & -37.05428 \times WT + 4.03094 \times 10^{-3} \times T_{ON} \times SV + 1.44031 \times 10^{-3} \times T_{OFF} \times V + 0.025620 \\ & \times I_P \times WT - 0.016321 \times T_{ON}^2 + 7.68448 \times 10^{-3} \times SV^2 - 9.07836 \times 10^{-4} I_P^2 + 12.97369 \times WT^2 \end{aligned} \quad (4)$$

3.3. ANN Performance

A total of fifty input–output patterns were investigated through the NN toolbox available in the MATLAB software. In general, the ANN model is supposed to be of the form: X−N_1−N_2−Y, where X is the number of neurons in the input layer, N_1 is the number of neurons in the first hidden layer, N_2 is the number of neurons in the second hidden layer, and Y represents the number of neurons in the output layer. Moreover, noise was added to the weights in order to encourage the stability of the NN structure that is to be optimized. The Levenberg–Marquardt (LM) training algorithm was used to train the feed forward back propagation network with the help of the tansig function. The tansig function used for training this neural network is given by tansig (n)= $2 \div \left(1 + e^{-2n}\right)^{-1}$. In this work, we chose five neurons in the input layer that corresponds to T_{ON}, T_{OFF}, SV, I_P, and WT and three neurons in the output layer corresponding to K_f, R_a, and MRR, as shown in Figure 3.

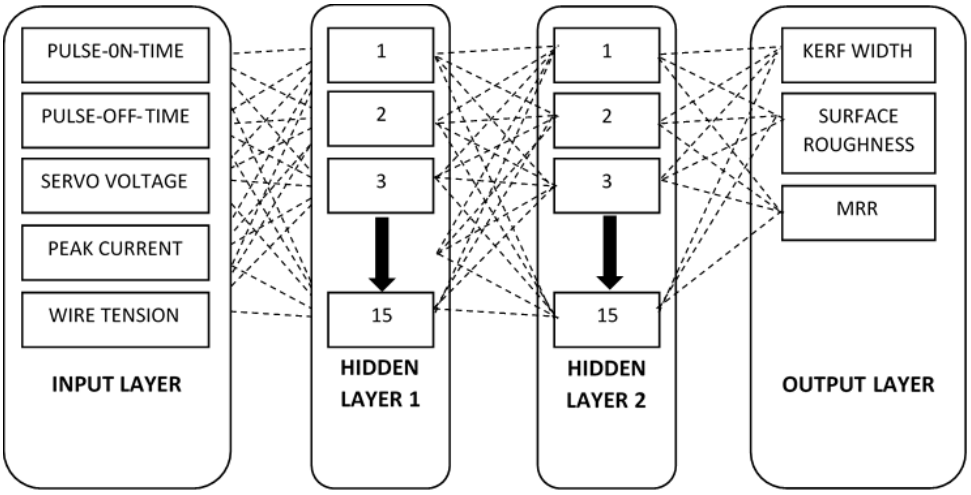

Figure 3. Artificial Neural Network architecture (5-N_1-N_2-3).

The performance of the network was judged on the basis of the Mean Square Error (MSE) which is given by the following equation.

$$MSE \;=\; \frac{1}{M \times N} \sum_{j=1}^{N} \sum_{i=1}^{M} \left(Y_i' - Y_i\right)^2 \quad (5)$$

where Y'_i is the experimental output of the ith neuron, Y_i is the predicted output of the ith neuron, N is the total number of training patterns, and M is the total number of neurons in the output layer [43].

Numerous trails were conducted by varying the number of neurons in the first layer to optimize the 5-N_1-3 NN structure. Based on the performance the number of neurons in the N_1 layer was finalised and then the neurons in the second hidden layer were varied from one to fifteen in order to optimize 5-13-N_2-3. This methodology was adopted to reduce the number of total combinations of neurons on both hidden layers by a significant amount from 225 to 30. For the first step, the performance of the 5-13-3 structure was found as optimum with 4.74% MSE. Then, while varying the neurons in the second hidden layer, the performance of the 5-13-15-3 structure was found as optimum with 1.49% MSE. The NN structure was trained more than once with minimal variation in weights in order to avoid the problems of local minima. Therefore, the 5-13-15-3 structure was selected for the prediction of the WEDM process performance in later sections. Data on the sensitivity of ANN's response to the number of neurons are presented in Table 8.

Table 8. ANN architecture performance while varying the number of neurons.

For hidden Layer = 1		For Hidden Layer = 2		
No. of Neurons	**MSE**	**No. of Neurons in the 1st Layer**	**No. of Neurons in the 2nd Layer**	**MSE**
1	1.103645	13	1	0.986389
2	0.337575	13	2	1.619909
3	0.219654	13	3	0.401487
4	0.146387	13	4	0.154014
5	0.124594	13	5	0.270056
6	0.150487	13	6	0.070328
7	0.145620	13	7	0.138533
8	0.077698	13	8	0.445419
9	0.049678	13	9	1.158510
10	0.088550	13	10	0.150517
11	0.090630	13	11	0.328056
12	2.448050	13	12	0.081355
13	0.047438	13	12	0.191720
14	0.155834	13	14	0.203620
15	4.100331	13	15	0.014916

3.4. Validation Experiments

Six additional experiments were performed using settings of input parameters that are different from the settings used in Table 4. Results of the validation experiments are presented in Table 9.

The predicted outcomes of these validation experiments obtained using RSM and ANN models were found to be in good agreement suggesting that the developed model can reliably be used for representing the experimental results. Moreover, MSE for prediction is also given in Table 8 and the ANN model outperformed the RSM model with a lower MSE of 1.41% than that of 6.33% of the RSM model.

Table 9. Comparison of predicted WEDM output parameters by RSM and ANN with experimental results, including absolute and percent errors.

S. No.	Input Parameters					Response Variables			Predicted Values						Absolute Error						Percentage Error					
									RSM			ANN			RSM			ANN			RSM			ANN		
	T_{ON}	T_{OFF}	V	I_P	T	K_f	R_a	MRR	K_f	R_a	MRR	K_f	R_a	MRR	K_f	R_a	MRR	K_f	R_a	MRR	K_f	R_a	MRR	K_f	R_a	MRR
1	100	50	60	150	1.3	0.338	2.12	5.50	0.359	2.30	5.90	0.343	2.17	5.60	0.020	0.180	0.399	0.004	0.051	0.104	6.0	8.4	7.2	1.4	2.4	1.8
2	110	50	40	180	1.1	0.378	2.97	6.33	0.405	3.21	6.82	0.383	3.03	6.43	0.026	0.241	0.489	0.004	0.056	0.105	7.1	8.1	7.7	1.2	1.8	1.6
3	120	40	40	150	1.5	0.381	3.06	7.82	0.411	3.30	8.42	0.386	3.12	7.94	0.030	0.240	0.597	0.005	0.059	0.123	7.9	7.8	7.6	1.3	1.9	1.5
4	105	40	50	120	1.3	0.349	1.13	5.83	0.379	1.23	6.30	0.359	1.16	5.97	0.030	0.096	0.477	0.009	0.023	0.146	8.6	8.4	8.1	2.8	2.1	2.5
5	110	60	60	140	1.5	0.355	2.47	8.57	0.385	2.67	9.25	0.362	2.52	8.73	0.029	0.201	0.682	0.006	0.043	0.165	8.3	8.1	7.9	1.9	1.7	1.9
6	120	60	50	180	1.4	0.368	2.86	5.73	0.410	3.16	6.30	0.380	2.96	5.89	0.042	0.300	0.565	0.011	0.102	0.156	11.4	10..4	9.8	3.1	3.5	2.7

3.5. Parametric Study Using the Developed ANN Model

The developed 5-13-15-3 ANN model was used to determine the effect of input process parameters on the response variables. While plotting the graphs for each individual parameter, other parameters were kept constant at zero level (see, Table 3).

3.5.1. Effect of Pulse-On-Time

From Figure 4a, it was observed that the K_f, R_a and MRR values increase with an increase in pulse-on-time value. An increase in T_{on} leads to an increase in the discharge energy melting more material from the work piece and thus increasing the K_f, R_a and MRR values [44]. In Figure 4b plotted between T_{ON} and R_a, it was observed that the surface roughness increases from 0.36 µm to 0.41 µm when the pulse-on-time increases from 100 µs to 120 µs. The increase in pulse-on-time also increases the crater size on the machine surface due to increased spark intensity thus leading to poor surface quality [45]. As shown in Figure 4c, the MRR increases with the increase in pulse-on-time till a pulse-on-time value of 115 µs and then slightly decreases at pulse-on-time value of 120 µs. The increase of MRR with increase of the pulse-on-time values is due to the higher thermal energy of the spark which melts and vaporizes consequently a larger amount of material from the plasma channel, hence leading to an increase in MRR [46].

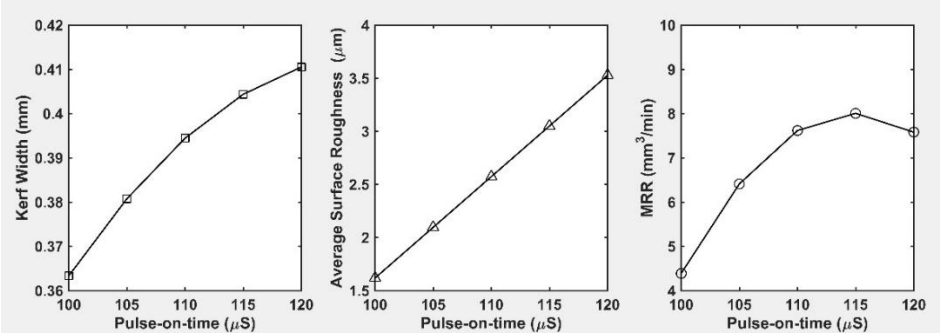

Figure 4. Effects of pulse-on-time (T_{ON}) on (**a**) kerf width, (**b**) surface roughness and (**c**) MRR.

3.5.2. Effect of Pulse-Off-Time

From the graph plotted in Figure 5a amid T_{OFF} and K_f, it appears that T_{OFF} has a negative impact on K_f i.e., K_f increases with the decrease in T_{OFF} and vice versa. Figure 5b shows a direct positive impact between T_{OFF} and R_a. As T_{OFF} increases, the flushing of the molten material significantly improves due to the increased time interval between two consecutive electrical discharges, thus improving the surface quality [44]. However, MRR decreases due to the reduced spark intensity at high T_{OFF}. Conversely, smaller T_{OFF} values tend to increase the spark intensity which melts and vaporizes a larger amount of material in the machining zone, thus increasing the MRR [47]. However, there is a critical value of T_{OFF} characterized by insufficient flushing of the molten material. This causes the formation of craters and micro-flaws on the machined surface thus increasing the surface roughness R_a.

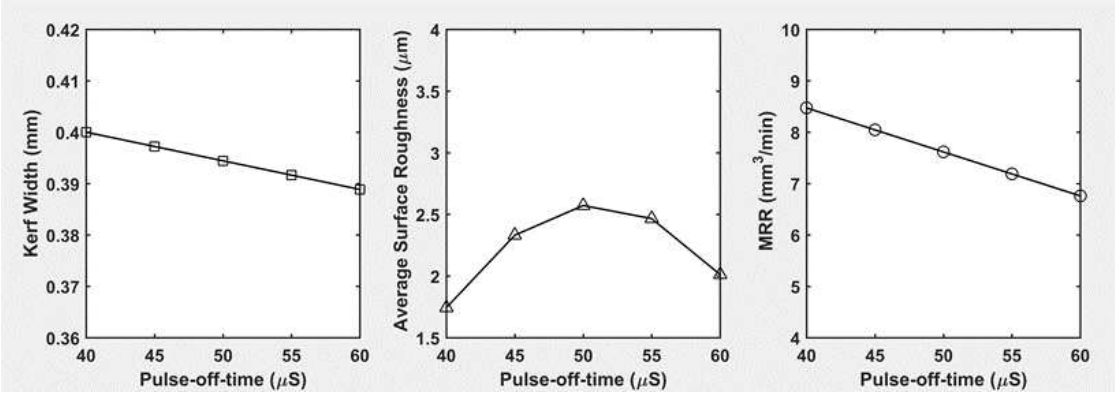

(**a**) (**b**) (**c**)

Figure 5. Effects of pulse-off-time (T_{OFF}) on (**a**) kerf width, (**b**) surface roughness and (**c**) MRR.

3.5.3. Effect of Servo-Voltage

The effect of servo-voltage on kerf width, R_a and MRR is shown in Figure 6a–c, respectively. The kerf width was not much influenced by the servo-voltage as seen from Figure 6a. It is apparent from Figure 6b that the R_a value initially decreases with increase in servo voltage up to a servo voltage value of 50 V and then increases with further increase in servo voltage. An increase in servo-voltage leads to higher values of MRR. It is known that higher voltages increase the spark discharge energy. This results in energy suspension amid the wire and work piece [46]. The higher evaporation rate is related to the larger discharge force exerted on the work piece area [48]. Thus, such energy dissolution leads to enhancement of the MRR and also contributes to decoration of the machined surface finish.

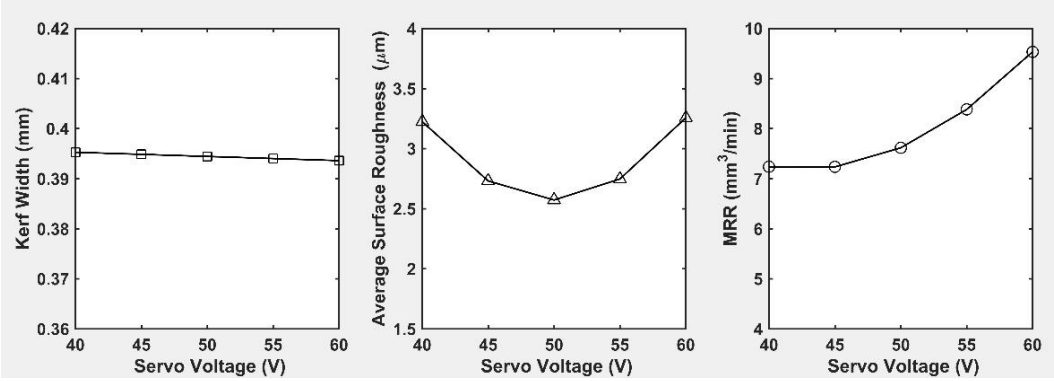

(**a**) (**b**) (**c**)

Figure 6. Effects of servo-voltage (SV) on (**a**) kerf width, (**b**) surface roughness, and (**c**) MRR.

3.5.4. Effect of Peak Current

The graph plotted in Figure 7b between I_P and R_a shows that the surface roughness increases from 2.4 µm to 2.7 µm with the increase in peak current value due to the increase in discharge energy. It is known that the discharge energy is proportional to the peak current [49]. At high values of peak current, continuous sparking occurs and hence MRR increases. This increase in discharge energy in turn leads to the melting of larger amounts of material and to increased kerf width, as can be seen from Figure 7a. The MRR was found to increase initially with an increase in peak current value till 150 A then tapers off.

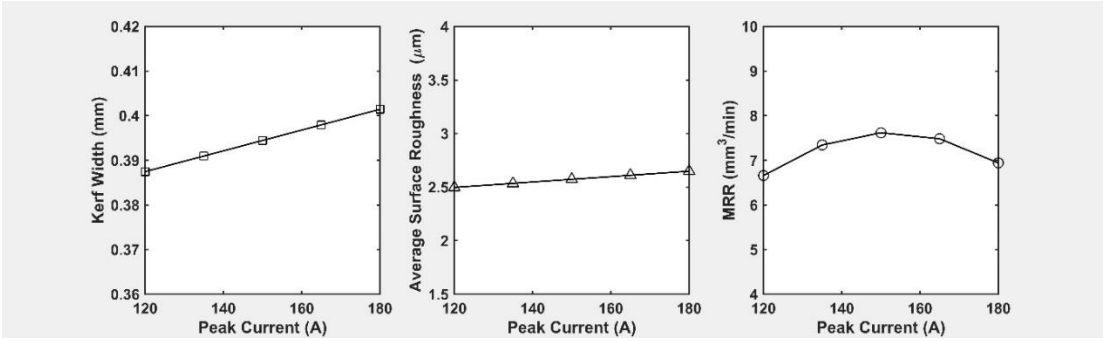

Figure 7. Effects of peak current (I_P) on (**a**) kerf width, (**b**) surface roughness, and (**c**) MRR.

3.5.5. Effect of Wire Tension

Figure 8a shows a graph plotted between WT and K_f. It was found that wire tension has a negligible impact on kerf width. Figure 8b shows that the effect of wire tension on surface quality is even less marked than the effect on kerf width. However, increasing wire tension allows mechanical vibrations to be reduced and thus wire deflection from its straight path to be minimized. Hence, the wire electrode keeps closer to its nominal (i.e., mean) position throughout the machining process. This contributes to enhance the MRR parameter (see Figure 8c).

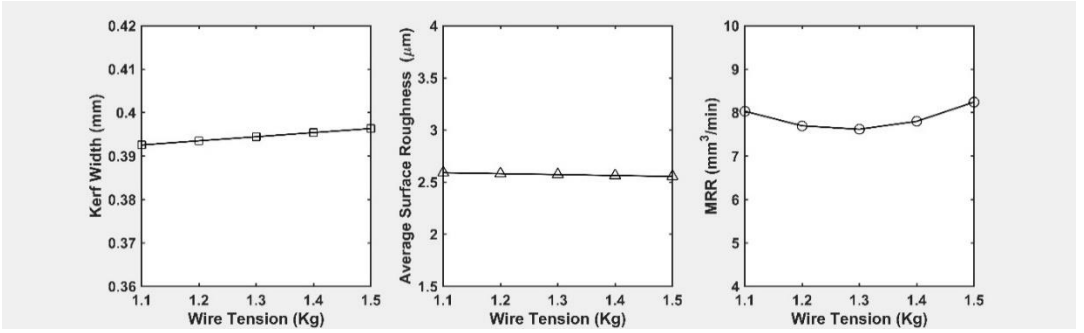

Figure 8. Effects of wire tension (WT) on (**a**) kerf width, (**b**) surface roughness, and (**c**) MRR.

3.6. Surface Morphology of the Wed Machined Specimens

The literature reports that the discharge energy mainly produces changes in the surface texture during the WEDM process. Hence, the surface quality of specimens machined using WEDM for different parametric settings was investigated (Figure 9). The material characterization depicts an uneven material deposition, presence of pockmarks and voids, globules of debris, and white layer formation. However, no surface cracking was witnessed. These patterns of machined specimens were obtained for different settings of parameters in such a manner as to detect the effect of pulse-on-time, sparking voltage, and pulse-off-time. The selected specimens were (i) Specimen of Experiment 3 (Figure 9a); (ii) Specimen of Experiment 48 (Figure 9b) and (iii) Specimen of Experiment 14 (Figure 9c).

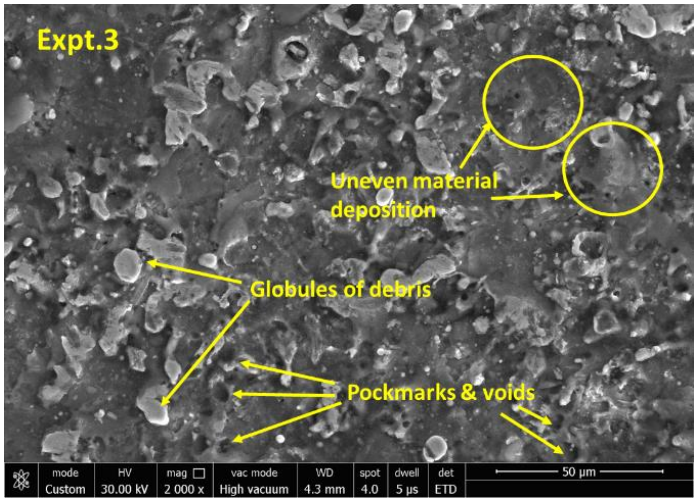

(**a**)

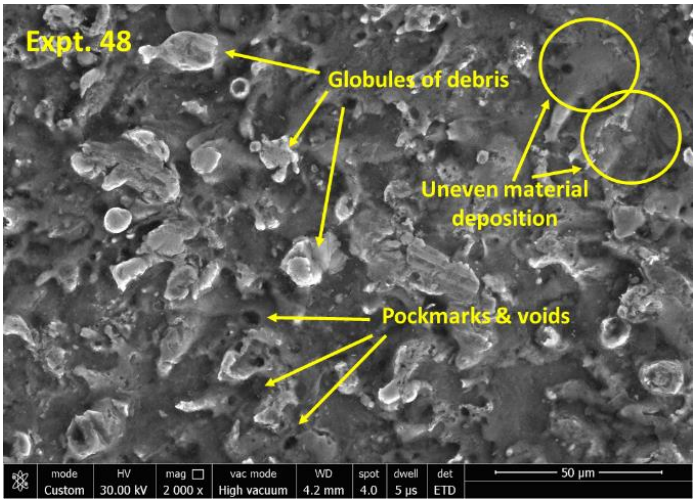

(**b**)

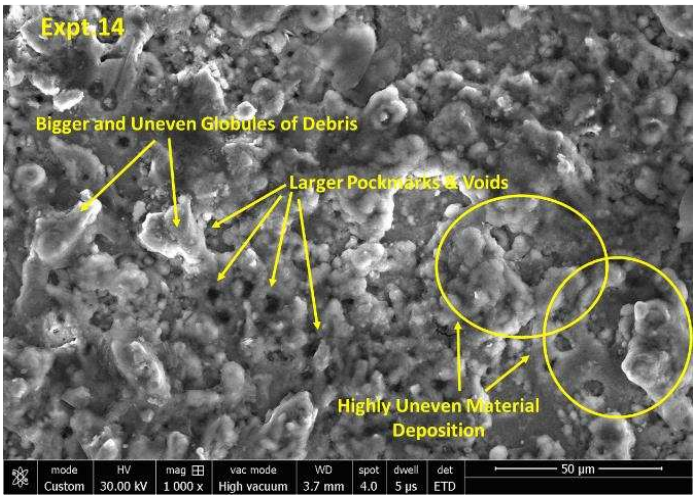

(**c**)

Figure 9. FESEM micrographs showing surface morphology of WEDM samples for different parametric settings. (**a**) Experiment 3: T_{ON} = 100 µs, T_{OFF} = 60 µs, SV = 40 V, I_P = 120 Amp, and WT = 1.1 kg. (**b**) Experiment 48: T_{ON} = 110 µs, T_{OFF} = 50 µs, SV = 50 V, I_P = 150 Amp, and WT = 1.1 kg. (**c**) Experiment 14: T_{ON} = 120 µs, T_{OFF} = 40 µs, SV = 60 V, I_P = 180 Amp, WT = 1.1 kg.

From Figure 9a,b, it can be observed that the increase in pulse-on-time from 100 µs to 110 µs, sparking voltage from 40 V to 50 V, and peak current from 120 to 150 A, resulted in enlargement of the size of globules of debris, bigger pockmarks and voids, and further uneven deposition of layers. Moreover, with increase in pulse-on-time, sparking voltage, and peak current, the discharge energy released per spark increases significantly. The increased discharge energy melts and vaporizes a larger amount of material from the plasma channel which helps in the formation of larger and deeper craters due to increased spark intensity [50]. A part of the melted materials is flushed away by pressurized dielectric fluid. However, the remaining molten material re-solidifies and forms globules of debris and pockmarks on the machined surface. It is suspected that the molten materials elemental composition has been altered during EDM action. Such phenomenon may occur when there is a high level of energy but not enough time to cool the surface and to remove the debris [51]. From Figure 9c, it is evident that for the largest values of pulse-on-time that is 120 µs, sparking voltage of 60 V, and peak current of 180 A, there is a significant increase in the size of globules of debris, pockmarks and voids, and further uneven deposition of layers due to increase in the thermal energy of the spark. It is evident from Figure 9a–c that a lower amount of globules, voids and pockmarks of smaller size form when the discharge energy is low. This is directly related to the crater size and amount of metal removed at low discharge energy. The size and number of globules, voids and pockmarks increase at higher discharge energy. The WEDM also attributes to modified surface layers of machined work pieces. These surface layers consist of a white layer (also known as the recast layer), heat affected zone and chemically affected zone with changes in the average chemical composition and possible phase changes. Typically, hardness of the white layer is higher than the bulk material due to the presence of oxides. However, this work did not study the influence of WEDM parameters on these surface layers of Inconel 718 and further study is required for such investigations.

3.7. NSGA-II Optimisation

The optimization problem was formulated with objectives to minimize the K_f and R_a and to maximize MRR. These goals are contradictory to each other and the function of pulse-on-time (T_{ON}), pulse-off-time (T_{OFF}), servo-voltage (SV), peak current (I_P) and wire tension (WT) were considered.

$$\begin{aligned} \textit{minimise } K_f &= f\left(T_{on}, T_{off}, SV,\ I_p,\ WT\right) \\ \textit{minimise } R_a &= f\left(T_{on}, T_{off}, SV,\ I_p,\ WT\right) \\ \textit{maximise } MRR &= -\textit{minimise } MRR = f\left(T_{on}, T_{off}, SV,\ I_p,\ WT\right) \end{aligned}$$

Subjected to constraints:

$$100 < T_{on} < 120$$

$$40 < T_{off} < 60$$

$$40 < V < 60$$

$$120 < I_p < 180$$

$$1.1 < WT < 1.5$$

The selected NSGA-II variables were identified on the basis of the literature and the characteristics of the current optimization problem to obtain optimal solutions with low computational effort: Maximum Number of Generations = 100, Total Population Size = 50, Mutation Probability = 0.25, Crossover Probability = 0.8. To determine the Total Population Size, sufficient optimization runs were conducted. After analyzing the results, it is found that the value of the objective functions attains its maximum value for a total population size of 50. Furthermore, it was observed that there was no appreciable change in the objective function value with further increase in total population size. Therefore, we selected a total population size of 50 for this research work. Crossover Probability for this research work is taken as 0.8, as it was observed that faster initial convergence was obtained for

the value of 0.8 after testing eight different values varying from 0.1 to 0.9. The Mutation Probability needs to be kept low in order to avoid random searches, but too low a mutation probability results in a local minimum/maximum. Therefore, a mutation probability of 0.25 was selected in this study so that the genetic algorithm avoids stopping at a local minimum/maximum. Figure 10 shows the Pareto front of the results in the exploration space for the optimization results. The NSGA-II yielded 18 optimal solutions which are listed in Table 10. Furthermore, it was also observed that there was a trade-off between MRR, kerf width, and surface roughness. i.e., no solution is better than any other solution and the decision maker will have to choose from the optimum results on the basis of particular requirements.

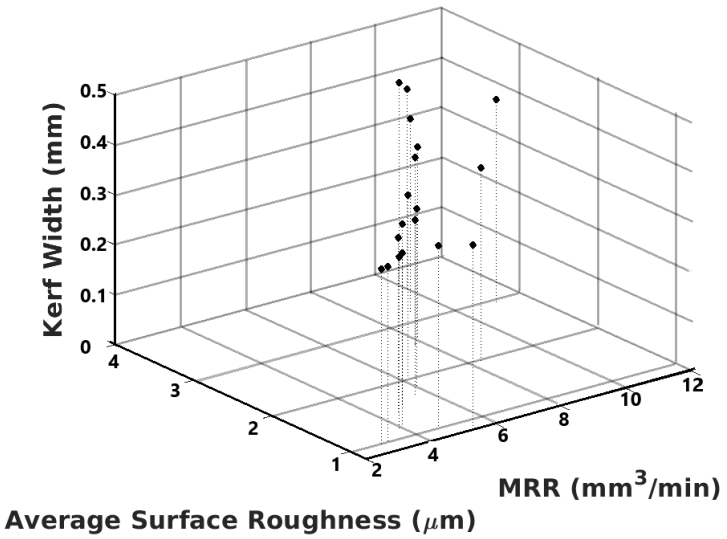

Figure 10. Pareto front of non-dominated solutions.

Table 10. Optimal combinations of WEDM parameters and non-dominated solutions.

S. No.	Optimum Combination of Parameters					Predicted Optimal Responses		
	Pulse on Time (μs)	Pulse off Time (μs)	Servo Voltage (V)	Peak Current (A)	Wire Tension (kg)	Kerf Width (mm)	Average Surface Roughness (μm)	MRR (mm^3/min)
1	115.7	41.3479	58.9851	145.6258	1.5	0.4115	2.9032	11.0445
2	116.1976	51.0227	58.8759	140.2582	1.002	0.4007	3.7455	10.081
3	115.7361	48.609	58.4004	140.9127	1.1499	0.403	3.5708	9.9281
4	111.8471	53.369	57.6318	139.7052	1.1846	0.3912	3.1399	8.982
5	106.2293	43.3575	55.8224	138.0302	1.4665	0.3886	1.9739	8.3452
6	109.0756	51.2509	54.952	135.5442	1.1557	0.3843	2.6745	8.0852
7	107.6299	54.3343	56.1504	137.6518	1.1792	0.3789	2.5472	7.7192
8	103.8108	55.7966	55.6415	136.7205	1.1733	0.3653	2.0421	6.2681
9	103.509	58.5855	56.0647	131.1638	1.1326	0.359	1.8143	5.9988
10	102.5863	59.2397	56.1829	129.3532	1.1186	0.3541	1.6625	5.5898
11	100.6012	40.2018	49.5448	125.1871	1.4991	0.3712	0.7983	5.3027
12	103.6348	58.6548	53.2785	125.4858	1.245	0.3623	1.5738	4.9978
13	100.4823	41.0112	49.6387	126.0315	1.2619	0.3636	1.0146	4.7551
14	100.8304	58.3529	54.7529	134.7287	1.1789	0.3524	1.4451	4.5571
15	100.1058	59.7993	54.683	127.479	1.1017	0.344	1.2261	4.1407
16	100.1064	59.6998	53.5976	126.8243	1.116	0.3449	1.1667	3.9059
17	100.1194	59.7852	51.1414	127.104	1.2612	0.3511	0.9925	3.1583
18	100.1884	59.7203	49.7307	123.9073	1.3032	0.3529	0.9621	2.8823

4. Conclusions

This work aimed to establish a predictive model for the wire electrical discharge machining process for machining Inconel 718. The experiments were performed using central composite design based on RSM to analyze the effects of various input parameter on the response variables. The ANN and RSM models were established to predict the process performance. The process optimization was further verified by applying the Non-dominated Sorting Genetic Algorithm (NSGA-II). The following conclusions were drawn based on the results obtained in this work.

1. ANOVA results indicate that T_{ON} has the highest impact on the machining of Inconel 718 by the WEDM process. Here, the percentage contributions of T_{ON} on K_f, R_a, and MRR were found to be 73.07%, 90.31%, and 46.99%, respectively. With an incrase in T_{ON}, the K_f, R_a, and MRR were found to increase due to the increase of discharge energy.
2. The results of ANOVA and analysis of experimental data indicate that the RSM models for K_f, R_a, and MRR are well fitted with the experimental values having a prediction error less than ±12%.
3. A robust process model was developed on the basis of a feed-forward back propagation neural network structure with 5-13-15-3 structure with minimum prediction MSE.
4. The confirmation experiments performed for the validation of both RSM and ANN models show that ANN, owing to its better modelling ability, is superior in giving appropriate and reliable predictions of K_f, R_a, and MRR compared to that of RSM models. The lower value of MSE for ANN (1.49%) than MSE for RSM (5.71%) further validates the better fitting of the neural network.
5. The surface morphology of WEDM machined samples shows the presence of a larger size of globules of debris, bigger pockmarks and voids, and further uneven deposition of layers for high discharge energy settings.

Author Contributions: Conceptualization, V.L.; Formal analysis, P.S., V.L.; Methodology, P.S.; Writing—original draft, V.S., D.R.U.; Writing—review, & editing, C.I.P. All authors have read and agreed to the published version of the manuscript.

Funding: This research received no external funding.

Conflicts of Interest: The authors declare no conflict of interest.

References

1. Venkatesan, K. The study on force, surface integrity, tool life and chip on laser assisted machining of inconel 718 using Nd:YAG laser source. *J. Adv. Res.* **2017**, *8*, 407–423. [CrossRef] [PubMed]
2. Nalbant, M.; Altın, A.; Gökkaya, H. The effect of cutting speed and cutting tool geometry on machinability properties of nickel-base Inconel 718 super alloys. *Mater. Des.* **2007**, *28*, 1334–1338. [CrossRef]
3. Chalisgaonkar, R.; Kumar, J. Multi-response optimization and modeling of trim cut WEDM operation of commercially pure titanium (CPTi) considering multiple user's preferences. *Eng. Sci. Technol. Int. J.* **2015**, *18*, 125–134. [CrossRef]
4. Sharma, N.; Khanna, R.; Gupta, R.D. WEDM process variables investigation for HSLA by response surface methodology and genetic algorithm. *Eng. Sci. Technol. Int. J.* **2015**, *18*, 171–177. [CrossRef]
5. Najafi, F.T. The computer in the construction industry. *Comput. Struct.* **1991**, *41*, 1125–1132. [CrossRef]
6. Tilekar, S.; Das, S.S.; Patowari, P.K. Process Parameter Optimization of Wire EDM on Aluminum and Mild Steel by Using Taguchi Method. *Procedia Mater. Sci.* **2014**, *5*, 2577–2584. [CrossRef]
7. Tosun, N.; Cogun, C.; Tosun, G. A study on kerf and material removal rate in wire electrical discharge machining based on Taguchi method. *J. Mater. Process. Technol.* **2004**, *152*, 316–322. [CrossRef]
8. Hewidy, M.S.; El-Taweel, T.A.; El-Safty, M.F. Modelling the machining parameters of wire electrical discharge machining of Inconel 601 using RSM. *J. Mater. Process. Technol.* **2005**, *169*, 328–336. [CrossRef]
9. Mahapatra, S.S.; Patnaik, A. Optimization of wire electrical discharge machining (WEDM) process parameters using Taguchi method. *Int. J. Adv. Manuf. Technol.* **2006**, *34*, 911–925. [CrossRef]
10. Kumar, K.; Agarwal, S. Multi-objective parametric optimization on machining with wire electric discharge machining. *Int. J. Adv. Manuf. Technol.* **2011**, *62*, 617–633. [CrossRef]
11. Sarkar, S.; Mitra, S.; Bhattacharyya, B. Parametric analysis and optimization of wire electrical discharge machining of γ-titanium aluminide alloy. *J. Mater. Process. Technol.* **2005**, *159*, 286–294. [CrossRef]
12. Kuriakose, S.; Mohan, K.; Shunmugam, M.S. Data mining applied to wire-EDM process. *J. Mater. Process. Technol.* **2003**, *142*, 182–189. [CrossRef]
13. Manna, A.; Bhattacharyya, B. Taguchi and Gauss elimination method: A dual response approach for parametric optimization of CNC wire cut EDM of PRAlSiCMMC. *Int. J. Adv. Manuf. Technol.* **2005**, *28*, 67–75. [CrossRef]

14. Bobbili, R.; Madhu, V.; Gogia, A.K. Modelling and analysis of material removal rate and surface roughness in wire-cut EDM of armour materials. *Eng. Sci. Technol. Int. J.* **2015**, *18*, 664–668. [CrossRef]
15. Patil, N.G.; Brahmankar, P.K. Some studies into wire electro-discharge machining of alumina particulate-reinforced aluminum matrix composites. *Int. J. Adv. Manuf. Technol.* **2009**, *48*, 537–555. [CrossRef]
16. Yadav, R.N.; Yadava, V. Multiobjective optimization of slotted electrical discharge abrasive grinding of metal matrix composite using artificial neural network and nondominated sorting genetic algorithm. *Proc. Inst. Mech. Eng. Part B: J. Eng. Manuf.* **2013**, *227*, 1442–1452. [CrossRef]
17. Samanta, B.; Erevelles, W.; Omurtag, Y. Prediction of workpiece surface roughness using soft computing. *Proc. Inst. Mech. Eng. Part B: J. Eng. Manuf.* **2008**, *222*, 1221–1232. [CrossRef]
18. Biswas, R.; Kuar, A.S.; Biswas, S.K.; Mitra, S. Artificial neural network modelling of Nd:YAG laser microdrilling on titanium nitride—Alumina composite. *Proc. Inst. Mech. Eng. Part B: J. Eng. Manuf.* **2009**, *224*, 473–482. [CrossRef]
19. Ramakrishnan, R.; Karunamoorthy, L. Modeling and multi-response optimization of Inconel 718 on machining of CNC WEDM process. *J. Mater. Process. Technol.* **2008**, *207*, 343–349. [CrossRef]
20. Saha, P.; Singha, A.; Pal, S.K.; Saha, P. Soft computing models based prediction of cutting speed and surface roughness in wire electro-discharge machining of tungsten carbide cobalt composite. *Int. J. Adv. Manuf. Technol.* **2007**, *39*, 74–84. [CrossRef]
21. Khan, I.A.; Rajput, T.S. Modeling of wire electrical discharge machining of alloy steel (HCHCr). *Int. J. Precis. Eng. Manuf.* **2012**, *13*, 1989–1995. [CrossRef]
22. Shandilya, P.; Jain, P.K.; Jain, N.K. Prediction of surface roughness during wire electrical discharge machining of SiCp/6061 Al metal matrix composite. *Int. J. Ind. Syst. Eng.* **2012**, *12*. [CrossRef]
23. Zhang, G.; Zhang, Z.; Guo, J.; Ming, W.; Li, M.; Huang, Y. Modeling and Optimization of Medium-Speed WEDM Process Parameters for Machining SKD11. *Mater. Manuf. Process.* **2013**, *28*, 1124–1132. [CrossRef]
24. Ugrasen, G.; Ravindra, H.V.; Prakash, G.V.N.; Keshavamurthy, R. Process Optimization and Estimation of Machining Performances Using Artificial Neural Network in Wire EDM. *Procedia Mater. Sci.* **2014**, *6*, 1752–1760. [CrossRef]
25. Vates, U.K.; Singh, N.K.; Singh, R.V. Modelling of Process Parameters on D2 Steel using Wire Electrical Discharge Machining with combined approach of RSM and ANN. *Int. J. Sci. Eng. Res.* **2014**, *8*, 2026–2035.
26. Shakeri, S.; Ghassemi, A.; Hassani, M.; Hajian, A. Investigation of material removal rate and surface roughness in wire electrical discharge machining process for cementation alloy steel using artificial neural network. *Int. J. Adv. Manuf. Technol.* **2015**, *82*, 549–557. [CrossRef]
27. Jafari, R.; Kahya, M.; Oliaei, S.N.B.; Ünver, H.Ö.; Özyurt, T.O. Modeling and analysis of surface roughness of microchannels produced by μ-WEDM using an ANN and Taguchi method. *J. Mech. Sci. Technol.* **2017**, *31*, 5447–5457. [CrossRef]
28. Singh, B.; Misra, J.P. Surface finish analysis of wire electric discharge machined specimens by RSM and ANN modeling. *Measurement* **2019**, *137*, 225–237. [CrossRef]
29. Mukhopadhyay, A.; Barman, T.; Sahoo, P.; Davim, J. Modeling and Optimization of Fractal Dimension in Wire Electrical Discharge Machining of EN 31 Steel Using the ANN-GA Approach. *Materials* **2019**, *12*, 454. [CrossRef]
30. Khan, M.A.R.; Rahman, M.M.; Kadirgama, K. An experimental investigation on surface finish in die-sinking EDM of Ti-5Al-2.5Sn. *Int. J. Adv. Manuf. Technol.* **2015**, *77*, 1727–1740. [CrossRef]
31. Chaudhary, T.; Siddiquee, A.N.; Chanda, A.K. Effect of wire tension on different output responses during wire electric discharge machining on AISI 304 stainless steel. *Def. Technol.* **2019**, *15*, 541–544. [CrossRef]
32. Unune, D.R.; Mali, H.S. Artificial neural network–based and response surface methodology–based predictive models for material removal rate and surface roughness during electro-discharge diamond grinding of Inconel 718. *Proc. Inst. Mech. Eng. Part B: J. Eng. Manuf.* **2016**, *230*, 2082–2091. [CrossRef]
33. Mazaheri, H.; Ghaedi, M.; Ahmadi Azqhandi, M.H.; Asfaram, A. Application of machine/statistical learning, artificial intelligence and statistical experimental design for the modeling and optimization of methylene blue and Cd(ii) removal from a binary aqueous solution by natural walnut carbon. *Phys. Chem. Chem. Phys.* **2017**, *19*, 11299–11317. [CrossRef] [PubMed]
34. Ranganathan, S.; Senthilvelan, T.; Sriram, G. Evaluation of Machining Parameters of Hot Turning of Stainless Steel (Type 316) by Applying ANN and RSM. *Mater. Manuf. Process.* **2010**, *25*, 1131–1141. [CrossRef]

35. Zopf, C.; Kaliske, M. Numerical characterisation of uncured elastomers by a neural network based approach. *Comput. Struct.* **2017**, *182*, 504–525. [CrossRef]
36. Pradhan, B.B.; Bhattacharyya, B. Modelling of micro-electrodischarge machining during machining of titanium alloy Ti-6Al-4V using response surface methodology and artificial neural network algorithm. *Proc. Inst. Mech. Eng. Part B: J. Eng. Manuf.* **2009**, *223*, 683–693. [CrossRef]
37. Chokshi, P.; Dashwood, R.; Hughes, D.J. Artificial Neural Network (ANN) based microstructural prediction model for 22MnB5 boron steel during tailored hot stamping. *Comput. Struct.* **2017**, *190*, 162–172. [CrossRef]
38. Unune, D.R.; Nirala, C.K.; Mali, H.S. ANN-NSGA-II dual approach for modeling and optimization in abrasive mixed electro discharge diamond grinding of Monel K-500. *Eng. Sci. Technol. Int. J.* **2018**, *21*, 322–329. [CrossRef]
39. Deb, K.; Pratap, A.; Agarwal, S.; Meyarivan, T. A fast and elitist multiobjective genetic algorithm: NSGA-II. *Ieee Trans. Evol. Comput.* **2002**, *6*, 182–197. [CrossRef]
40. Niu, X.; Wang, H.; Hu, S.; Yang, C.; Wang, Y. Multi-objective online optimization of a marine diesel engine using NSGA-II coupled with enhancing trained support vector machine. *Appl. Therm. Eng.* **2018**, *137*, 218–227. [CrossRef]
41. Unune, D.R.; Mali, H.S. Parametric modeling and optimization for abrasive mixed surface electro discharge diamond grinding of Inconel 718 using response surface methodology. *Int. J. Adv. Manuf. Technol.* **2017**, *93*, 3859–3872. [CrossRef]
42. Dabade, U.A.; Karidkar, S.S. Analysis of Response Variables in WEDM of Inconel 718 Using Taguchi Technique. *Procedia Cirp* **2016**, *41*, 886–891. [CrossRef]
43. Youssefi, S.; Emam-Djomeh, Z.; Mousavi, S.M. Comparison of Artificial Neural Network (ANN) and Response Surface Methodology (RSM) in the Prediction of Quality Parameters of Spray-Dried Pomegranate Juice. *Dry. Technol.* **2009**, *27*, 910–917. [CrossRef]
44. Singh, V.; Bhandari, R.; Yadav, V.K. An experimental investigation on machining parameters of AISI D2 steel using WEDM. *Int. J. Adv. Manuf. Technol.* **2017**, *93*, 203–214. [CrossRef]
45. Raju, P.; Sarcar, M.M.M.; Satyanarayana, B. Optimization of Wire Electric Discharge Machining Parameters for Surface Roughness on 316 L Stainless Steel Using Full Factorial Experimental Design. *Procedia Mater. Sci.* **2014**, *5*, 1670–1676. [CrossRef]
46. Vijayabhaskar, S.; Rajmohan, T. Experimental Investigation and Optimization of Machining Parameters in WEDM of Nano-SiC Particles Reinforced Magnesium Matrix Composites. *Silicon* **2018**. [CrossRef]
47. Kumar, H.; Manna, A.; Kumar, R. Modeling of Process Parameters for Surface Roughness and Analysis of Machined Surface in WEDM of Al/SiC-MMC. *Trans. Indian Inst. Met.* **2018**, *71*, 231–244. [CrossRef]
48. Kung, K.-Y.; Chiang, K.-T. Modeling and Analysis of Machinability Evaluation in the Wire Electrical Discharge Machining (WEDM) Process of Aluminum Oxide-Based Ceramic. *Mater. Manuf. Process.* **2008**, *23*, 241–250. [CrossRef]
49. Sreenivasa Rao, M.; Venkaiah, N. Experimental investigations on surface integrity issues of Inconel-690 during wire-cut electrical discharge machining process. *Proc. Inst. Mech. Eng. Part B: J. Eng. Manuf.* **2016**, *232*, 731–741. [CrossRef]
50. Unune, D.R.; Mali, H.S. Experimental investigation on low-frequency vibration-assisted μ-ED milling of Inconel 718. *Mater. Manuf. Process.* **2018**, *33*, 964–976. [CrossRef]
51. Torres, A.; Puertas, I.; Luis, C.J. Modelling of surface finish, electrode wear and material removal rate in electrical discharge machining of hard-to-machine alloys. *Precis. Eng.* **2015**, *40*, 33–45. [CrossRef]